IEEE Access
Multidisciplinary | Rapid Review | Open Access Journal

Received 3 June 2024, accepted 26 June 2024, date of publication 1 July 2024, date of current version 24 July 2024.

Digital Object Identifier 10.1109/ACCESS.2024.3421274

RESEARCH ARTICLE

Spectral Data Augmentation Using Deep Generative Model for Remote Chemical Sensing

JUNGJAE SON[1], HYUNG JOON BYUN[2], (Graduate Student Member, IEEE), MUNYEOL PARK[1], JEONGJAE HA[1], AND HYUNWOO NAM[1], (Member, IEEE)
[1]Chem-Bio Technology Center, Agency for Defense Development, Daejeon 34186, Republic of Korea
[2]Cornell Tech, New York, NY 10044, USA

Corresponding author: Hyunwoo Nam (hyunwoonam@add.re.kr)

This work was supported by the Agency for Defense Development funded by the Korean Government under Grant 915043101.

ABSTRACT The critical role of a remote chemical sensing using a Fourier Transform Infrared (FT-IR) spectrometer has been emphasized for detecting lethal chemicals in the atmosphere. To enhance standoff detection capabilities, acquiring adequate gas spectral data is crucial for training and optimizing detection algorithms across diverse outdoor scenarios. However, the collection of outdoor infrared spectra with a number of conditions is constrained owing to uncontrolled weather factors including a temperature and humidity, leading to impaired reliability of the data. In addressing outdoor data acquisition challenges, we introduced a data augmentation method using a conditional CycleGAN. This technique utilizes spectral data obtained exclusively under controlled laboratory conditions. The proposed deep generative model takes as input the background spectrum, which is concatenated with two critical attributes: the temperature difference between the target substance and the background, and pathlength concentration. Subsequently, the model computes a brightness temperature spectrum for a gas against a specific background, employing SF_6 as the target chemical gas. The validity of the generated data was assessed using two detection algorithms: the Pearson Correlation Coefficient and Adaptive Subspace Detector. In addition, the accuracy performance of detectors trained with the augmented dataset was compared and evaluated against those trained with the pure dataset. The results demonstrated that the model can simulate gas spectra onto unseen background spectra and enhance the chemical sensing database, and it can contribute to data augmentation for improving the performance of chemical gas detection systems.

INDEX TERMS Brightness temperature spectrum, data augmentation, deep generative model, FT-IR spectroscopy, generative adversarial network, remote chemical sensing.

I. INTRODUCTION

Chemical gases such as chemical warfare agents (CWAs) and toxic industrial chemicals (TICs) pose a significant risk of causing severe casualties and fatalities. However, their odorless and colorless characteristics pose challenges for human nervous system recognition [1]. In order to safeguard individuals from hazardous substances, extensive research has investigated methods for detecting and identifying chemical gases [2], [3], [4], [5]. Especially, a remote chemical sensing is a promising technology for mitigating operator and equipment contamination without direct contact.

Capturing and analyzing a spectrum of chemical gas is one of the methods for a long-range chemical detection. Toxic chemicals, in particular, exhibit distinctive spectral patterns primarily in the long-wave infrared ($7 \sim 14\mu m$) region. These patterns serve as unique fingerprints for identification. To acquire the spectrum, a passive Fourier Transform Infrared (FT-IR) spectroscopy has been investigated since it is feasible to be optimized for a mobile surveillance application.

The associate editor coordinating the review of this manuscript and approving it for publication was Chengpeng Hao.

Typically, a prediction accuracy improves with an increasing number of reference datasets for the inference scheme. However, obtaining sufficient spectral data remains challenging owing to the difficulty of conducting outdoor experiments under controlled ambient conditions. In outdoor environments, precise control over gas plume temperature, background conditions, plume concentration, and dispersion is challenging due to weather uncertainties. In addition, conducting outdoor experiments with toxic chemicals is restricted by the elevated risk of personnel injury and testing region contamination.

This study introduces a methodology of synthesizing a pure gas spectrum under the controlled laboratory condition and various natural background spectrum using a conditional CycleGAN. We trained the Generative Adversarial Network (GAN) model with its attributes to control the generation of the chemical spectrum. As a result, we demonstrated the feasibility of integrating our generated spectra with an unseen background spectrum. In order to validate realism and rationality, we evaluated the generated spectrum using two detection algorithms: the Pearson Correlation Coefficient (PCC) and an Adaptive Subspace Detector (ASD). Finally, to demonstrate that the data generated by the proposed deep generative model can lead to improvements of the performance in actual chemical gas detection systems, we conducted the comparative analysis of detectors trained on the augmented dataset and the pure dataset, respectively.

The proposed deep generative model is capable of achieving a meaningful contribution to addressing data acquisition challenges, which is additionally leading to improvement of the experimental environment, condition, and safety. Moreover, it is anticipated to have a potential with its generalizability and scalability for all data-driven technologies to offer more constructive contributions in the field of contemporary science and technology.

II. RELATED WORKS

A. INFRARED RADIATION EMULATION

Models that emulate the interplay between infrared radiation and outdoor environments, including the toxic chemicals have been studied. Notably, a simplified model of atmospheric composition, also known as 3-Layer Model [6], facilitates gas spectrum generation through mathematical modeling. This model assumes a linear combination of atmospheric radiation, gas plume, and background, yielding a realistic gas spectrum. However, obtaining essential atmospheric parameters for modeling, including atmospheric transmittance, poses challenges. This requirement necessitates the use of an additional model, such as MODTRAN [7], which significantly complicates the augmentation of spectral data. Moreover, even with such a spectrum, errors in linear approximation cannot be entirely avoided.

B. DEEP GENERATIVE MODELS

To address these limitations of the linear mathematical generation model, deep generative models have been suggested. Generative Adversarial Network (GAN) proposed by Goodfellow et al. [8] has a potential to augment a database with realistic and meaningful data while involving nonlinearity. To apply the data augmentation technique to various tasks, several forms of GAN have been developed by modifying the network architecture or adjusting the loss function such as cGAN [9], WGAN [10], DCGAN [11], and CycleGAN [12].

C. DATA AUGMENTATION USING GAN

Augmented data using deep generative models has been demonstrated to enhance performance in recognition and detection. For instance, Kukreja et al. [13] achieved improved accuracy in vehicle number plate recognition by training a CNN with an augmented dataset using a GAN. Wang et al. [14] devised a deep generative model based on DCGAN to address the scarcity of training samples for palmprint recognition. Luo and Lu [15] introduced a conditional Wasserstein GAN (CWGAN) for EEG data augmentation to enhance EEG-based emotion recognition in terms of its accuracy. Patel et al. [16] improved the F1 score of automatic modulation classification with the augmented dataset using a conditional GAN (cGAN). Sandfort et al. [17] enhanced robustness and generalizability of organ segmentation in CT segmentation tasks with the dataset extended utilizing CycleGAN. Motamed et al. [18] suggested IAGAN to detect a pneumonia and COVID-19 in chest X-ray images with higher sensitivity, specificity, and accuracy. Waheed et al. [19] employed CovidGAN to enhance CNN-based COVID-19 detection using synthetic X-ray images. LeafGAN proposed by Cap et al. [20] increased a detection reliability for a practical plant disease diagnosis.

Deep generative models have also contributed to a development in image-to-image translation area. For example, AugGAN devised by Huang et al. [21] demonstrated effective image translation while maintaining characteristic consistency through training YOLO and Faster R-CNN detectors. In addition, Lin et al. [22] introduced cd-GAN, a conditional image translation method that preserves domain-independent features while reconstructing images in the target domain. Furthermore, Lu et al. [23] investigated a conditional CycleGAN for generating high-resolution face images from low-resolution inputs. Notably, they achieved precise control over facial attributes by incorporating an additional attribute vector into the input.

III. METHODS

A. BRIGHTNESS TEMPERATURE SPECTRUM

Spectral data were acquired using a Miniaturized Stand-off Chemical Agent Detector (MSCAD), a custom built passive FT-IR spectroscopy in the long-wave infrared (LWIR) region. The system relies solely on reflected radiation, without an active light source. The Michelson interferometer captures the spectrum as light traverses it, equidistantly from the moving mirror. Subsequently, the sampled data in

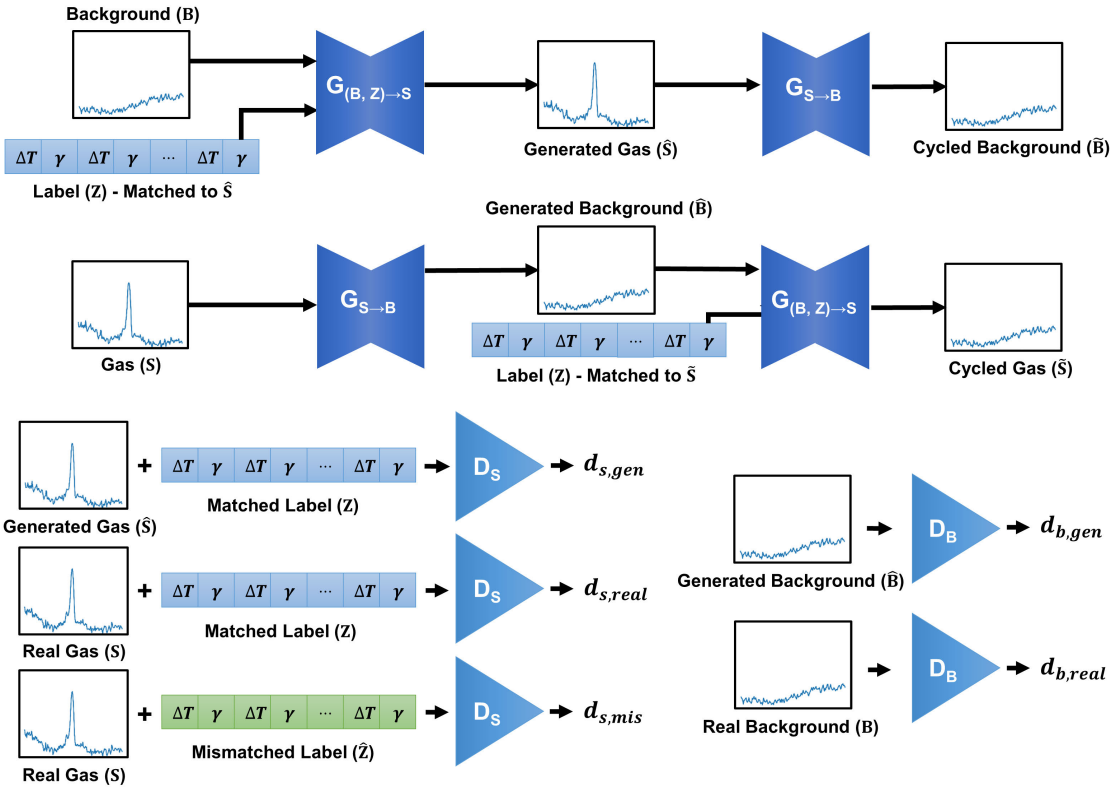

FIGURE 1. Network architecture of proposed conditional CycleGAN for domain to domain translation of brightness temperature spectrum.

spatial domain are converted into the spectral radiance in wavenumber domain by a Fast Fourier Transform.

The spectral radiance of black body $B(\bar{\nu},\ T)$ is represented as Planck function,

$$B(\bar{\nu},\ T) = \frac{2hc^2\bar{\nu}^3}{\exp(hc\bar{\nu}/k_BT) - 1}, \tag{1}$$

where $\bar{\nu}$ is the wavenumber, T is the temperature, h is the Planck constant, k_B is the Boltzmann constant, and c is the speed of light according to the black body radiation theory. For a certain material with temperature T and its spectral radiance $L(\bar{\nu},\ T)$, the emissivity of the material is defined as a ratio of the spectral radiance of the material and the black body,

$$\epsilon(\bar{\nu}) = \frac{L(\bar{\nu},\ T)}{B(\bar{\nu},\ T)}. \tag{2}$$

However, identifying gas absorption patterns from the spectral radiance poses challenges due to its wavenumber and temperature dependence. Consequently, a stable baseline for comparison with the reference database is lacking. To address this, we employ a spectral brightness temperature $T(\bar{\nu},\ L)$ derived using the inverse Planck function,

$$T(\bar{\nu},\ L) = \frac{hc\bar{\nu}}{k_B \ln(2hc^2\bar{\nu}^3/L + 1)}. \tag{3}$$

In the LWIR region, when operating the remote chemical sensing, most common Earth background material exhibit emissivity values within the range $0.9 \sim 1$, with spectral radiance comparable to that of the black body [24]. If a chemical substance exists in the atmosphere, the spectral brightness temperature exhibits a specific peak, contrasting with the pure background spectrum. The location of the peak depends on the chemical substance type, while its height primarily relies on two attributes: the temperature difference (ΔT) between background and the substance, and the concentration along the line of sight of the spectroscopy, also known as pathlength concentration (γ) [6]. In this study, the data acquisition, model training, and model validation were conducted by varying these two parameters.

B. CONDITIONAL CYCLEGAN FOR SPECTRAL DATA AUGMENTATION

The objective of the deep generative model is to generate the gas spectrum given the background. In addition, the generated gas spectrum is controlled by its attributes. Thus, the conditional CycleGAN [23] architecture was applied to domain-to-domain translation. Let the background domain as B and the gas spectrum domain as S. The translation $B \rightarrow S$ takes attributes vector z of the gas spectrum. Thus, we denote generators as $G_{(B,\ Z)\rightarrow S}$ and $G_{S\rightarrow B}$ and discriminators as D_S and D_B. The network design of the generative model is illustrated in figure 1.

The adversarial loss $\mathcal{L}(G_{(B,\,Z)\to S},\ D_S)$ is defined as,

$$\mathcal{L}(G_{(B,Z)\to S}, D_S) = \min_G \max_D \{\mathbb{E}_{s,z}[\log D_S(s,z)] + \mathbb{E}_{b,z}[\log(1 - D_S(G_{(B,Z)\to S}(b,z),z))]\}, \tag{4}$$

and adversarial loss $\mathcal{L}(G_{S\to B}, D_B)$ is defined as,

$$\mathcal{L}(G_{S\to B}, D_B) = \min_G \max_D \{\mathbb{E}_b[\log D_B(b)] + \mathbb{E}_s[\log(1 - D_B(G_{S\to B}(s)))]\}. \tag{5}$$

The cycle consistency loss $\mathcal{L}_c(G_{(B,\,Z)\to S}, G_{S\to B})$ is defined as,

$$\begin{aligned}\mathcal{L}_c(G_{(B,\,Z)\to S}, G_{S\to B}) &= \|G_{S\to B}(G_{(B,Z)\to S}(b,z)) - b\|_1 \\ &\quad + \|G_{(B,Z)\to S}(G_{S\to B}(s)) - s\|_1.\end{aligned} \tag{6}$$

The identity loss $\mathcal{L}_i(G_{(B,\,Z)\to S}, G_{S\to B})$ is defined as,

$$\begin{aligned}\mathcal{L}_i(G_{(B,\,Z)\to S}, G_{S\to B}) &= \|G_{(B,Z)\to S}(s,z) - s\|_1 \\ &\quad + \|G_{S\to B}(b) - b\|_1.\end{aligned} \tag{7}$$

Thus, the total loss is

$$\begin{aligned}\mathcal{L}(G_{(B,Z)\to S}, G_{S\to B}, D_B, D_S) &= \mathcal{L}(G_{(B,Z)\to S}, D_S) + \mathcal{L}(G_{S\to B}, D_B) \\ &\quad + \lambda_c \mathcal{L}_c(G_{(B,\,Z)\to S}, G_{S\to B}) \\ &\quad + \mathcal{L}_i(G_{(B,\,Z)\to S}, G_{S\to B}).\end{aligned} \tag{8}$$

The value of λ_c was 1 in this study.

We also induced the generative model to ultimately generate gas spectra matching the input attributes by considering the mismatched attributes during the training. Therefore, the gas discriminator D_S of the network is trained to classify real spectrum with incorrect labels as spurious. Consequently, the gas discriminator loss $\mathcal{L}_{D_S}$ is calculated as

$$\mathcal{L}_{D_S} = \log(d_{s,real}) + \frac{1}{2}\log[(1 - d_{s,gen})(1 - d_{s,mis})], \tag{9}$$

and the background discriminator loss $\mathcal{L}_{B_S}$ is calculated as

$$\mathcal{L}_{B_S} = \log(d_{b,real}) + \log(1 - d_{b,gen}). \tag{10}$$

C. DETECTION ALGORITHMS

1) BACKGROUND REMOVAL

In order to validate the generated dataset, detection algorithms were used. The prerequisite for running the algorithms is to get pure gas spectrum which does not contain the background information. A Linear Subspace Model was employed to achieve the pure gas spectrum assuming that an incident spectrum x is a linear combination of pure gas signal, background signal, and noise. Let x be denoted as

$$\mathbf{x} = \mathbf{s}g + \mathbf{K}_{bg}\mathbf{y}_{bg} + \mathbf{n}, \tag{11}$$

where $\mathbf{x}$ is the fingerprint spectrum of gas, g is the pure gas signal intensity, $\mathbf{K}_{bg}$ is a matrix of background information, $\mathbf{y}_{bg}$ is a vector of background coefficients, and $\mathbf{n}$ is a Gaussian noise. Given $\mathbf{K} = [\mathbf{s}, \mathbf{K}_{bg}]$ and $\mathbf{y} = [g, \mathbf{y}_{bg}^T]^T$, the signal is denoted as

$$\mathbf{x} = \mathbf{K}\mathbf{y} + \mathbf{n}. \tag{12}$$

By applying least square method, the approximate signal coefficient vector $\hat{\mathbf{y}}$ is,

$$\hat{\mathbf{y}} = (\mathbf{K}^T\mathbf{K})^{-1}\mathbf{K}^T\mathbf{x} = [\hat{g}, \hat{\mathbf{y}}_{bg}^T]^T. \tag{13}$$

Thus, the approximate pure spectrum $\hat{\mathbf{p}}$ is obtained by,

$$\hat{\mathbf{p}} = \mathbf{x} - \mathbf{K}_{bg}\hat{\mathbf{y}}_{bg}, \tag{14}$$

which is subsequently compared against the database using the algorithms.

2) PEARSON CORRELATION COEFFICIENT

Assume a database spectrum $\mathbf{t} = (t_1, t_2, \ldots, t_n)$ of size n. The approximate pure spectrum $\hat{\mathbf{p}} = (\hat{p}_1, \hat{p}_2, \ldots, \hat{p}_n)$ is compared to t using Pearson Correlation Coefficient, which is defined as

$$T_{PCC} = \frac{n\Sigma t_i\hat{p}_i - \Sigma t_i \Sigma \hat{p}_i}{\sqrt{\Sigma t_i^2 - (\Sigma t_i)^2}\sqrt{\Sigma \hat{p}_i^2 - (\Sigma \hat{p}_i)^2}}. \tag{15}$$

The threshold of T_{PCC} for SF_6 to be detected is 0.89. This value was set according to the results of SF_6 detection experiments using a MSCAD prototype in Agency for Defense Development, South Korea.

3) ADAPTIVE SUBSPACE DETECTOR

Using the Linear Subspace Model, we assume two hypotheses H_0 and H_1, such that

$$\begin{aligned}H_0 &: \mathbf{x} = \mathbf{K}_{bg}\mathbf{y}_{bg} + \mathbf{n} \\ H_1 &: \mathbf{x} = \mathbf{s}g + \mathbf{K}_{bg}\mathbf{y}_{bg} + \mathbf{n},\end{aligned} \tag{16}$$

where H_0 represents the absence of the target gas, and H_1 represents the presence of the target gas. Since $\mathbf{n}$ follows a Gaussian distribution, the incident spectrum $\mathbf{x}$ is a random variable, such that

$$\begin{aligned}H_0 &: \mathbf{x} \sim N(\mathbf{K}_{bg}\mathbf{y}_{bg}, \sigma_0^2\mathbf{I}) \\ H_1 &: \mathbf{x} \sim N(\mathbf{K}\mathbf{y}, \sigma_1^2\mathbf{I}).\end{aligned} \tag{17}$$

Then, the Generalized Likelihood Ratio of the hypotheses is,

$$T_{ASD}(\mathbf{x}) = \frac{\mathbf{x}^T(\mathbf{P}_{\mathbf{K}_{bg}} - \mathbf{P}_{\mathbf{K}})\mathbf{x}}{\mathbf{x}^T\mathbf{P}_{\mathbf{K}}\mathbf{x}}, \tag{18}$$

where $\mathbf{P}_{\mathbf{K}} = \mathbf{I} - \mathbf{K}(\mathbf{K}^\mathbf{T}\mathbf{K})^{-\mathbf{1}}\mathbf{K}^\mathbf{T}$ and $\mathbf{P}_{\mathbf{K}_{bg}} = \mathbf{I} - \mathbf{K}_{bg}(\mathbf{K}_{bg}^T\mathbf{K}_{bg})^{-1}\mathbf{K}_{bg}^T$. The threshold of T_{ASD} for SF_6 to be detected is 1.0. This standard was also determined based on the findings from the SF_6 detection experiments using MSCAD.

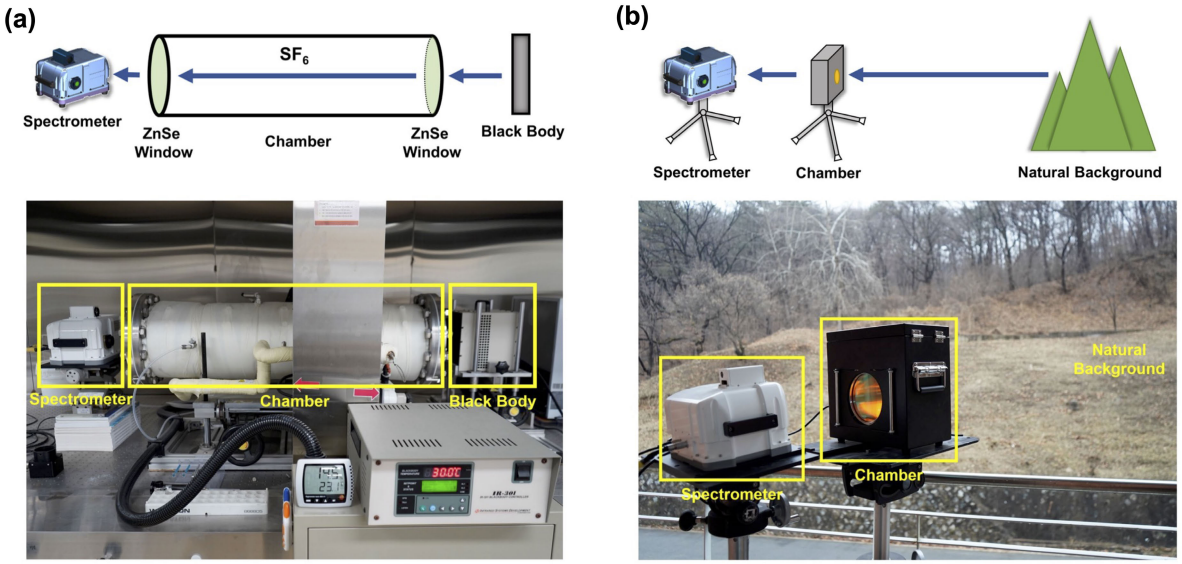

FIGURE 2. Configurations of the Spectrum acquisition experiment. (a) Laboratory spectrum acquisition with black body as the background. (b) Outdoor spectrum acquisition with natural background.

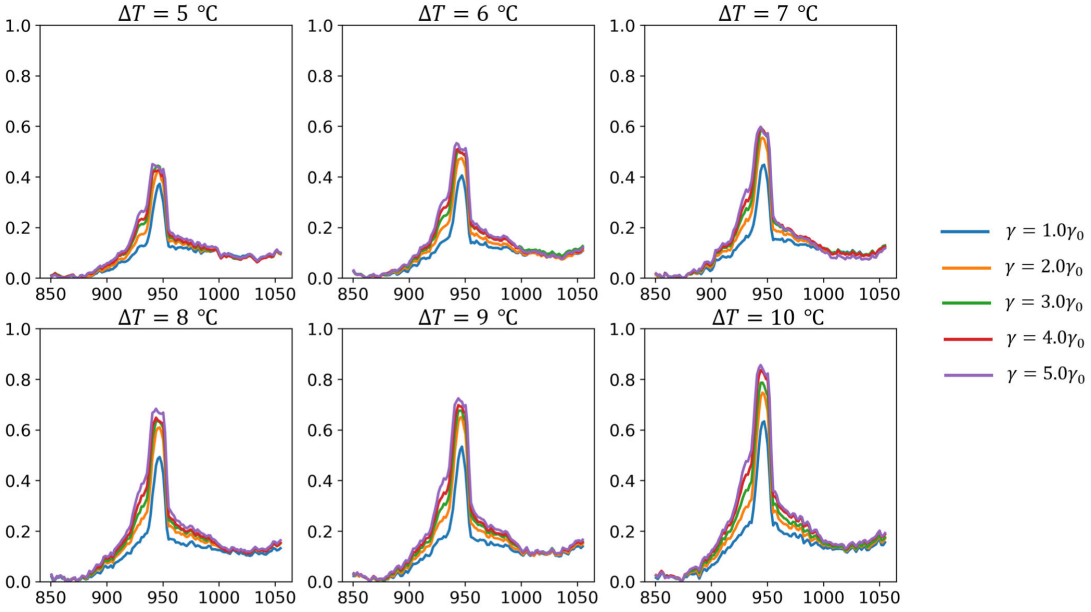

FIGURE 3. Samples of acquired training data with black body background. X-axis and Y-axis indicate wavenumber in units of cm^{-1} and normalized value of the spectral brightness temperature, respectively.

IV. EXPERIMENT

A. DATASET

1) DATA ACQUISITION

The training data were acquired in a laboratory environment, as shown in Figure 2(a). The target gas was a Sulfur Hexafluoride (SF_6). The FT-IR spectrometer occupied one side of a horizontal cylindrical chamber, with observation facilitated through a ZnSe window transparent in the IR region. A temperature-controlled black body was positioned on the opposite side of the chamber as background. The SF_6 gas inside the chamber was elevated to a temperature of $40°C$. The temperature range of the black body was systematically adjusted from $30°C$ to $35°C$ with $1°C$ interval, resulting in six distinct temperature difference (ΔT).

The pathlength concentration γ is calculated as

$$\gamma = c_{gas} \times L\,[mg/m^2]. \tag{19}$$

L represents the optical path length within the gas cloud, and c_{gas} denotes the mean gas concentration along this path. For simplicity, a constant $\gamma_0 = 172.55\ mg/m^2$ was introduced. The optical path length was a chamber length of $1m$ and the

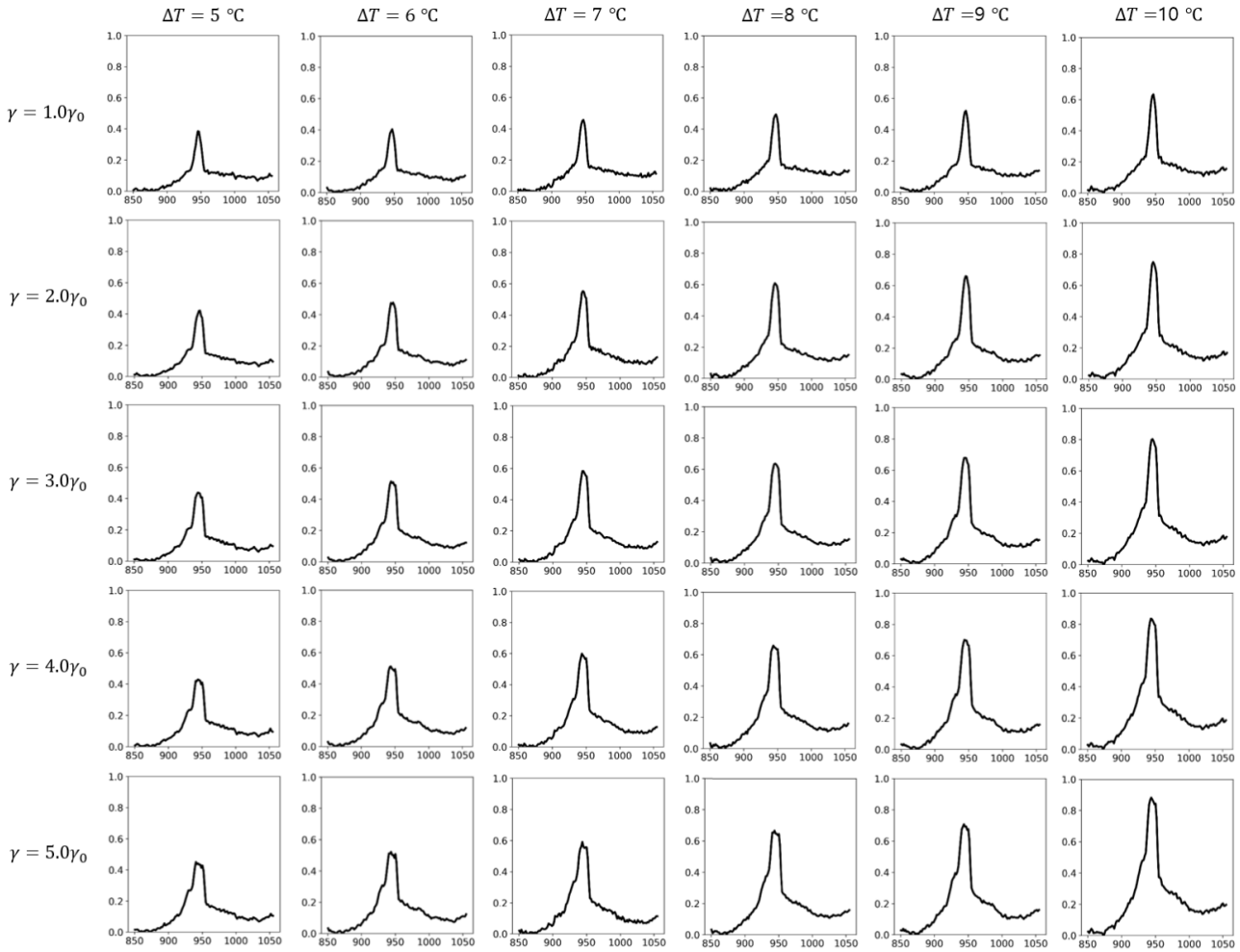

FIGURE 4. Samples of the generated brightness temperature spectra under different conditions with black body background. X-axis and Y-axis indicate wavenumber in units of cm^{-1} and normalized value of the spectral brightness temperature, respectively.

gas concentration was calculated using the ideal gas law:

$$c_{gas} = \frac{M_{gas}}{V_{chamber}} = \frac{M_w}{V_{chamber}} \times \frac{P_{gas}\, V_{gas}}{R\, T_{gas}}, \qquad (20)$$

where M_{gas} represents the mass of the gas, the molecular weight M_w of SF_6 is $146.055 g/mol$, the chamber volume $V_{chamber}$ is $0.0346185 m^3$, and the gas constant R is $0.08205 L \cdot atm/K \cdot mol$. Since gas was injected into the chamber from a tedlar bag using a gas-tight syringe at the laboratory temperature, the gas pressure P_{gas} was $1 atm$ and gas temperature T_{gas} was $298 K$. Twenty-five different pathlength concentration (γ) were considered by varying V_{gas} from $0.2 ml$ to $5.0 ml$ with $0.2 ml$ intervals.

Therefore, the dataset was constructed using data obtained from 25×6 experimental conditions and the total size of the dataset was 75, 000. The training and validation sets were divided at a ratio of $8 : 2$. Figure 3 depicts samples of obtained training data on a black body background.

The test data were acquired in the outdoor environment with natural backgrounds, as depicted in Figure 2(b). The selected backgrounds contained four types that are commonly found in nature, which are earthy ground, concrete walls, asphalt, and tree-covered mountains. The portable chamber containing SF_6, where $V_{chamber}$ is $0.002934016 m^3$ and L is $0.146 m$, was positioned before the spectrometer. The gas injection procedure mirrored that of the training data acquisition. The gas quantity was manipulated to achieve three distinct path length concentrations: $0.4\gamma_0$, $1.0\gamma_0$, and $2.8\gamma_0$. Additionally, we controlled the chamber temperature relative to the natural background temperature, considering three different temperature differences: $8°C$, $10°C$, and $12°C$. The background temperature was measured using an IR thermometer.

2) DATA PREPROCESSING

The background and gas spectrum were truncated to the wavenumber range of [850, 1050] to achieve a size of 128, since the dominant peak of SF_6 is observed to be located around $940 cm^{-1}$. The spectrum was then subtracted by the minimum value of the spectrum and divided by 10 to obtain

a range in $[0, 1]$. The attribute vector z consists of two attributes: temperature difference $\Delta T \in \mathbb{N}$ and pathlength concentration $\gamma \in \mathbb{R}$. The tuple of $(\Delta T,\ \gamma)$ was repeated 64 times to create z with a size of 128. This z was subsequently concatenated with the background spectrum. Thus, the input size of $G_{(B,\ Z)\to S}$ was 256.

B. NETWORK SETTINGS

The network architecture is depicted in Figure 1. The generators consisted of symmetrical fully-connected layers with dimensions of $64, 64, 32, 32$ for the first half and $32, 32, 64, 64$ for the second half with ReLU activation. The discriminators consisted of fully-connected layers with size of 256, 256, 64, 32 with leaky ReLU activation. The kernels in the layers were applied with L2 regularization with a factor of 0.00001. Adam optimizer was employed with adaptive learning rate using cosine decay schedule to stabilize the training steps. The number of epochs was 700 and size of the minibatch was 256.

C. EXPERIMENTAL RESULTS

1) TRAINING RESULTS

Initially, we analyzed the controllability of brightness temperature spectrum generation based on the given attributes, which consisted of the temperature difference and pathlength concentration. Figure 4 illustrates the brightness temperature spectra produced by the deep generative model, the conditional CycleGAN, across varying temperature difference and the pathlength concentration. The spectra described the shape of SF_6 that has a distinctive peak near $940cm^{-1}$. The generated spectra at lower concentrations had sharper and lower peak. In contrast, thicker and higher peak was formed under the condition with the high SF_6 concentration. In addition, a convex in the positive direction appeared near $930cm^{-1}$, which is positioned at the left slope of the peak near $940cm^{-1}$. These peak characteristics were observed in the spectra acquired during the experiment with a black body background, as shown in Figure 3, where height of the peak had a positive correlation with temperature difference and pathlength concentration.

Subsequently, two detection algorithms were employed to validate the generated spectra against a standard SF_6 database. The detection scores presented in table 1 were ordered by varying the input concentration of SF_6, which were averaged over the temperature difference values. The scores in table 2 were ordered by the temperature difference between the gas and the background, which were averaged over the pathlength concentrations. Notably, the Pearson Correlation Coefficient scores exceeded 0.89 and the Adaptive Subspace Detector scores surpassed 1.0. These thresholds are based on the algorithms of in-operation spectrometer prototype of the Agency for Defense Development.

As evidenced by the similarity in peak shapes and results of the detection algorithms, it is clear that the deep generative network has been trained properly to generate valid spectrum with controlled attributes.

TABLE 1. Detection scores of the generated brightness temperature spectrum with black body background by varying γ.

γ	$0.4\gamma_0$	$0.8\gamma_0$	$1.2\gamma_0$	$1.6\gamma_0$	$2.0\gamma_0$	$2.4\gamma_0$
T_{PCC}	0.906	0.987	0.985	0.980	0.973	0.966
T_{ASD}	17.383	24.97	18.037	13.588	10.064	7.845
γ	$2.8\gamma_0$	$3.2\gamma_0$	$3.6\gamma_0$	$4.0\gamma_0$	$4.4\gamma_0$	$4.8\gamma_0$
T_{PCC}	0.959	0.951	0.943	0.934	0.923	0.912
T_{ASD}	6.341	5.287	4.498	3.837	3.260	2.828

TABLE 2. Detection scores of the generated brightness temperature spectrum with black body background by varying ΔT.

$\Delta T(^\circ C)$	5	6	7	8	9	10
T_{PCC}	0.911	0.922	0.959	0.956	0.959	0.963
T_{ASD}	7.492	6.815	10.050	10.356	11.283	10.652

2) TEST RESULTS

The performance of the conditional CycleGAN model, in generating a brightness temperature spectrum using unseen background spectrum, was evaluated. The test dataset featured four different natural backgrounds including mountains, earthy ground, asphalt, and concrete walls, which were absent from the training dataset. The trained model computed infrared spectrum for each background, assuming the presence of SF_6. Figure 5 illustrates samples of the generated spectra alongside their corresponding ground-truth spectra, considering three distinct path length concentrations (γ) and three different temperature differences (ΔT) between the gas and background. The pathlength concentration was set to one of $0.4ml$, $1.0ml$, or $2.8ml$ and the temperature difference was set to one of $8^\circ C$, $10^\circ C$, or $12^\circ C$.

Figure 5(a), 5(b), 5(c), and 5(d) present the generated brightness temperature spectra with the background of mountain, earthy ground, asphalt, and concrete wall, respectively. From this figure, the similarity between the spectra generated by the model and the ground truth spectra can be assessed for each case. The trend of a positive correlation between the characteristics of the peak and two parameters, pathlength concentration and temperature difference, was observed across all backgrounds in the test dataset. Remarkably, despite excluding temperature differences exceeding $10^\circ C$ during training, the generated spectra for a $12^\circ C$ of temperature difference closely resembled the ground truth data. This result implies that the GAN model successfully trained the generalized peak characteristics based on the given attributes. However, an offset discrepancy existed in the vicinity of $1,000cm^{-1}$. All four backgrounds exhibit emissivities within the range of 0.9 or higher. Therefore, the brightness temperature spectra of each background have similarity to the black body radiation. However, there are unavoidable differences which caused the offset. This phenomenon became pronounced when a background spectrum exhibited steeper concavity distinct from that of the black body. If the training data include brightness temperature spectra

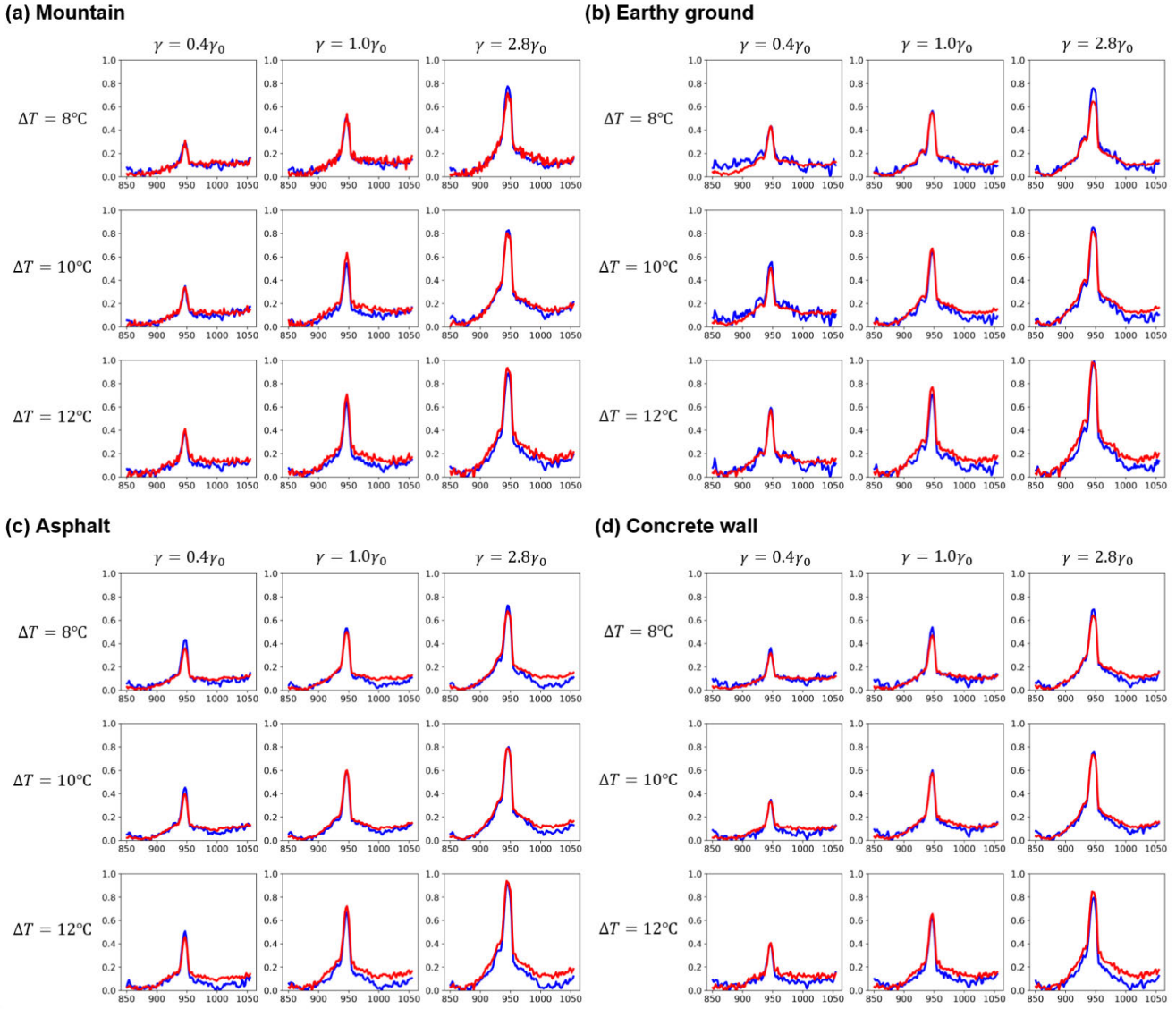

FIGURE 5. Generated brightness temperature spectra with 4 different natural backgrounds, (a) Mountain, (b) Earthy ground, (c) Asphalt, and (d) Concrete wall. The red line and the blue line indicate generated spectrum and reference spectrum, respectively. X-axis and Y-axis of each graph indicate wavenumber in units of cm^{-1} and normalized value of the spectral brightness temperature, respectively.

across diverse backgrounds and the generative model learns translations for various background domains, the conditional CycleGAN can have a potential to mitigate these limitations.

The validity of the generated spectra with the natural backgrounds was confirmed using the detection algorithms, as listed in table 3. This table presents the detection scores for each attribute condition in the form of (Pearson Correlation Coefficient / Adaptive Subspace Detector). These metrics demonstrate the realism of the generated data. The scores in the table are averaged based on the number of samples. The scores from both detection algorithms satisfied the detection criteria, where the threshold of Pearson Correlation Coefficient and Adaptive Subspace Detector are 0.89 and 1.0, respectively. In all cases, the Pearson Correlation Coefficient exceeded 0.927, and the Adaptive Subspace Detector surpassed 3.407. These results demonstrate the capability of the model to emulate the gas spectra onto unseen background spectrum and augment the database for chemical sensing by training the GAN model using laboratory experimental spectral data. Thus, the deep generative model facilitates scalable generation of a brightness temperature spectrum reflecting the intention of the user by adjusting the background and attributes. Moreover, this findings demonstrate the potential of this model to contribute to data augmentation for improving the performance of chemical gas detection.

Subsequently, the performance of the deep generative model was compared to the baseline model in order to establish the superiority of the proposed model. The baseline model was implemented by merely adding the brightness

TABLE 3. Detection scores (Pearson Correlation Coefficient / Adaptive Subspace Detector) of the generated brightness temperature spectra with natural backgrounds, (a) Mountain, (b) Earthy ground, (c) Asphalt, and (d) Concrete wall.

(a)

$\Delta T(^\circ C)$ \ γ	$0.4\gamma_0$	$1.0\gamma_0$	$2.8\gamma_0$
8	0.982 / 15.434	0.986 / 19.939	0.927 / 3.407
10	0.988 / 23.408	0.989 / 25.516	0.975 / 10.472
12	0.965 / 7.542	0.967 / 7.873	0.963 / 7.067

(b)

$\Delta T(^\circ C)$ \ γ	$0.4\gamma_0$	$1.0\gamma_0$	$2.8\gamma_0$
8	0.992 / 34.622	0.988 / 22.784	0.966 / 7.757
10	0.984 / 17.171	0.983 / 15.613	0.974 / 10.409
12	0.959 / 6.278	0.958 / 6.200	0.954 / 5.592

(c)

$\Delta T(^\circ C)$ \ γ	$0.4\gamma_0$	$1.0\gamma_0$	$2.8\gamma_0$
8	0.990 / 28.919	0.985 / 18.262	0.943 / 4.422
10	0.988 / 21.993	0.987 / 20.918	0.978 / 12.258
12	0.960 / 6.537	0.963 / 6.998	0.960 / 6.503

(d)

$\Delta T(^\circ C)$ \ γ	$0.4\gamma_0$	$1.0\gamma_0$	$2.8\gamma_0$
8	0.989 / 25.070	0.987 / 20.463	0.940 / 4.245
10	0.987 / 21.720	0.987 / 21.604	0.977 / 11.652
12	0.962 / 6.868	0.963 / 7.080	0.961 / 6.600

TABLE 4. Comparison results of detection scores, Pearson Correlation Coefficient and Adaptive Subspace Detector, between the proposed deep generative model, conditional CycleGAN, and the baseline model, with four natural backgrounds, (a) Mountain, (b) Earthy ground, (c) Asphalt, and (d) Concrete wall.

(a)

Score \ Model	Baseline	CycleGAN	Improvement
T_{PCC}	0.899	0.971	+8.07%
T_{ASD}	8.817	13.406	+52.05%

(b)

Score \ Model	Baseline	CycleGAN	Improvement
T_{PCC}	0.910	0.973	+6.91%
T_{ASD}	11.741	14.047	+19.64%

(c)

Score \ Model	Baseline	CycleGAN	Improvement
T_{PCC}	0.881	0.973	+10.43%
T_{ASD}	7.762	14.090	+81.53%

(d)

Score \ Model	Baseline	CycleGAN	Improvement
T_{PCC}	0.873	0.973	+11.35%
T_{ASD}	4.378	13.922	+218.00%

temperature spectrum of SF_6 gas and the background. We measured the average Pearson Correlation Coefficient score and average Adaptive Subspace Detector score of the spectra generated by the conditional CycleGAN model and the baseline model with respect to the reference spectrum data. The table 4 presents the results of this comparative analysis. The results indicate that, for all natural backgrounds utilized in this study, the proposed deep generative model generates spectra that are closer to the reference compared to the baseline model. The deep generative model exhibited +8.070%, +6.906%, +10.428%, and +11.352% improvement in Pearson Correlation Coefficient scores compared to the baseline for mountain, earthy ground, asphalt, and concrete wall, respectively. In addition, the model demonstrated +52.05%, +19.64%, +81.53%, and +218.00% improvement in Adaptive Subspace Detector scores compared to the baseline for each mentioned backgrounds, respectively.

D. MODEL EFFECTIVENESS VALIDATION

The effectiveness of the trained deep generated model was validated by testing the effectiveness of the augmented dataset on the gas detection. In order to address our proposed conditional CycleGAN model effectively improves the performance of chemical gas detection systems by augmenting the dataset, tests for an impact of the artificial spectrum data on performance of detectors were conducted. We compared the accuracy of the detectors trained with pure dataset and augmented dataset, respectively. Support Vector Machine-based detector and Deep Neural Network-based detector were used for the tests. The pure dataset is composed of data obtained exclusively from the actual experiments, without incorporating any data generated by the deep generative model. In contrast, the augmented dataset refers to the pure dataset supplemented with brightness temperature spectrum data generated by the developed deep generative model. To evaluate the effects of data augmentation, we compared the performance of two detectors trained with the pure dataset, the 150% augmented dataset, and the 200% augmented dataset. This comparative analysis was performed using accuracy and ROC curve. The results of this experiment can be observed in a Figure 6.

The pure dataset comprises 500 brightness temperature spectra acquired from actual experiments. In the dataset, 250 spectra correspond to scenarios with the presence of SF6 gas, while the remaining 250 spectra correspond to scenarios without the gas. The 150% augmented dataset consists of the pure dataset of 500 spectra supplemented with an additional 250 spectra generated by the deep generative model. The 200% augmented dataset comprises the pure dataset with an additional 500 generated spectra. The performance of the two detectors, each trained on datasets of sizes 500, 750, and 1000, was evaluated using test dataset. The test dataset consists of data with randomly assigned

(a) Mountain

Detector \ Dataset	Pure Dataset	150% Augmented Dataset	200% Augmented Dataset
SVM	0.725	0.803	0.814
DNN	0.785	0.810	0.903

(b) Earthy ground

Detector \ Dataset	Pure Dataset	150% Augmented Dataset	200% Augmented Dataset
SVM	0.680	0.825	0.914
DNN	0.685	0.783	0.905

(c) Asphalt

Detector \ Dataset	Pure Dataset	150% Augmented Dataset	200% Augmented Dataset
SVM	0.780	0.823	0.930
DNN	0.810	0.900	0.948

(d) Concrete wall

Detector \ Dataset	Pure Dataset	150% Augmented Dataset	200% Augmented Dataset
SVM	0.650	0.777	0.825
DNN	0.700	0.780	0.905

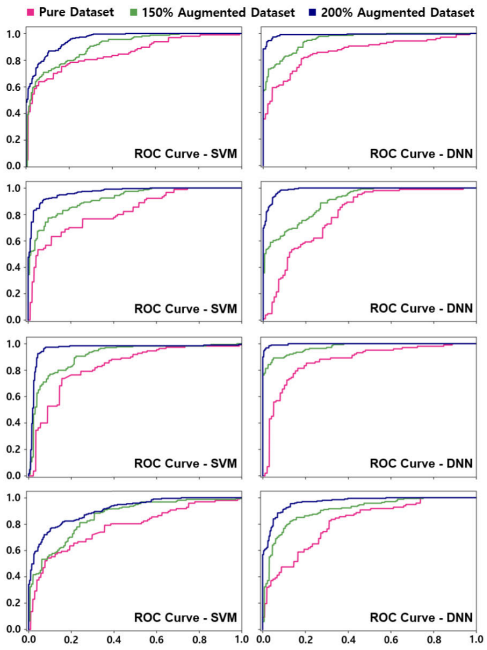

FIGURE 6. Accuracy and ROC curve of two detectors, Support Vector Machine (SVM) and Deep Neural Network (DNN), trained with pure dataset, 150% augmented dataset, and 200% augmented dataset, for each natural backgrounds, (a) Mountain, (b) Earthy ground, (c) Asphalt, and (d) Concrete wall. In the graphs on the right side, pink line, green line, and blue line indicate ROC curve of detectors trained with pure dataset, 150% augmented dataset, and 200% augmented dataset, respectively.

conditions, specifically within a pathlength concentration range of $0.0005\gamma_0$ to $0.001\gamma_0$ and a temperature difference range of $5°C$ to $10°C$. To facilitate effective comparative analysis, the test dataset was constructed using data from scenarios with low SF_6 gas concentrations. In scenarios with high SF_6 concentrations, the detectors consistently demonstrated high accuracy regardless of the training dataset size or the type of detector, thereby obscuring any meaningful effects of the data augmentation.

The results in Figure 6 demonstrate an improvement in accuracy due to the data augmentation using the proposed deep generative model. Moreover, as data augmentation is applied, the ROC curve shifts towards the upper left corner. Thus, it is clearly confirmed that the spectral data augmentation using the deep generative model effectively improves the performance of the chemical gas sensing systems.

V. DISCUSSION

When conducting research on machine learning-based generative models, it is essential to discuss which models are suitable depending on the situation, conditions, and objectives. In this study, which involves developing a model to generate spectra that vary according to temperature and concentration conditions across different backgrounds, a conditional CycleGAN was used. Other promising candidate methods capable of performing similar tasks include transformer-based methods such as diffusion model. Therefore, it is meaningful to consider the transformer-based model and perform a comparative analysis between transformer-based diffusion model and CycleGAN, when conducting research on the deep generative models.

A. SUITABILITY FOR UNPAIRED DATASET LEARNING

CycleGAN exhibits suitability for learning from unpaired datasets according to [12]. Since datasets are usually unpaired in real-world, especially in the field of remote chemical detection, CycleGAN is anticipated to fit into generative model for scarce and scattered dataset. The conditional CycleGAN model proposed in this study ultimately aims to generate paired data using unpaired datasets for specific backgrounds, temperatures, and path length concentrations. CycleGAN learns mappings between two different domains without requiring paired data for training. This can be achieved by leveraging the cycle consistency loss.

B. COMPUTATIONAL EFFICIENCY

The transformer-based diffusion model can be another suitable deep generative model. However, it is known to be computationally complex. Self-attention mechanism in the transformer models to calculate interactions between each element in the input sequence requires high memory bandwidth. Furthermore, transformer models typically have a large number of layers and parameters.

Compared to the transformer models, CycleGAN holds an advantage in terms of computational cost. This characteristic enhances its feasibility and applicability, in resource-constrained scenarios such as miniaturized edge devices for chemical gas detection. In our study, the proposed model utilizes a generator with only 8 layers of fully-connected

layers and a discriminator with 5 layers of fully-connected layers, requiring fewer learnable parameters compared to transformer-based models. Additionally, the total training time amounted to approximately only 3 hours for 700 epochs with NVIDIA GeForce RTX 2080 Ti, further highlighting its computational efficiency. Moreover, during the inference, only the generator layers are needed to create the spectra, which significantly reduces the number of parameters and computation efforts. In fact, according to [25], it can be observed that CycleGAN used approximately 33% less training time and 59% fewer parameters compared to UVCGAN, a transformer-based deep generative model.

VI. CONCLUSION

We proposed a method for augmenting spectral brightness temperature data using conditional CycleGAN where the generated spectrum relies on the attributes of the gas, specifically the temperature difference and pathlength concentration. To train the network, we acquired spectra under controlled experimental settings by varying the temperatures of the chamber and black body, and adjusting the concentration of SF_6. With the obtained dataset, we trained the network with the emphasis on its controllability of the peak characteristics using the concatenated attributes vector. According to the training results, the network successfully learned the generation mechanisms of SF_6, demonstrating the learned patterns of morphological trends based on changes in attributes. In addition, the generated spectra were validated by testing them on the detection algorithms. Specifically, the network successfully produced SF_6 spectra on novel natural backgrounds not included in the training data. Furthermore, a simulating capability for a $12°C$ temperature difference case demonstrated control over previously unseen attributes. Finally, the value of data augmentation using the proposed deep generative model was demonstrated as the performance of detectors trained on the augmented dataset surpassed that of detectors trained on the pure dataset.

Therefore, this model enables the rational and proper generation of brightness temperature spectra across various conditions, including different backgrounds, temperatures, and concentrations of chemical gases. This showed the feasibility of spectral data augmentation of the chemical gases using the conditional CycleGAN model. Obtaining a sufficient amount of data is important to ensure adequate performance of the tasks involving the detection and identification of chemical gases. However, achieving this in practice is challenging. Consequently, it is anticipated that this data augmentation model can contributes to enhancing the performance of the remote chemical sensing using FT-IR spectroscopy, mitigating several practical difficulties.

Future works may include the development of deep generative models for multiple types of chemical gas spectrum which involves many-to-many domain translations. This data augmentation is anticipated to enhance detection performance across a wider range of backgrounds and chemical substances. A comparative analysis of several generative machine learning models for data augmentation can also be considered as a meaningful future study.

ACKNOWLEDGMENT

(Jungjae Son and Hyung Joon Byun contributed equally to this work.)

REFERENCES

[1] V. Kumar, H. Kim, B. Pandey, T. D. James, J. Yoon, and E. V. Anslyn, "Recent advances in fluorescent and colorimetric chemosensors for the detection of chemical warfare agents: A legacy of the 21st century," *Chem. Soc. Rev.*, vol. 52, no. 2, pp. 663–704, 2023.

[2] S. Fan, G. Zhang, G. H. Dennison, N. FitzGerald, P. L. Burn, I. R. Gentle, and P. E. Shaw, "Challenges in fluorescence detection of chemical warfare agent vapors using solid-state films," *Adv. Mater.*, vol. 32, no. 18, May 2020, Art. no. 1905785.

[3] C. E. Davidson, M. M. Dixon, B. R. Williams, G. K. Kilper, S. H. Lim, R. A. Martino, P. Rhodes, M. S. Hulet, R. W. Miles, A. C. Samuels, P. A. Emanuel, and A. E. Miklos, "Detection of chemical warfare agents by colorimetric sensor arrays," *ACS Sensors*, vol. 5, no. 4, pp. 1102–1109, Apr. 2020.

[4] W.-Q. Meng, A. C. Sedgwick, N. Kwon, M. Sun, K. Xiao, X.-P. He, E. V. Anslyn, T. D. James, and J. Yoon, "Fluorescent probes for the detection of chemical warfare agents," *Chem. Soc. Rev.*, vol. 52, no. 2, pp. 601–662, 2023.

[5] H. J. Byun and H. Nam, "Autonomous control of unmanned aerial vehicle for chemical detection using deep reinforcement learning," *Electron. Lett.*, vol. 58, no. 11, pp. 423–425, May 2022.

[6] D. Manolakis, S. Golowich, and R. S. DiPietro, "Long-wave infrared hyperspectral remote sensing of chemical clouds: A focus on signal processing approaches," *IEEE Signal Process. Mag.*, vol. 31, no. 4, pp. 120–141, Jul. 2014.

[7] A. Berk, L. S. Bernstein, and D. C. Robertson, *Modtran: A Moderate Resolution Model for Lowtran*. Burlington, MA, USA: Spectral Sciences Inc., 1987.

[8] I. Goodfellow, J. Pouget-Abadie, M. Mirza, B. Xu, D. Warde-Farley, S. Ozair, A. Courville, and Y. Bengio, "Generative adversarial nets," in *Proc. Adv. Neural Inf. Process. Syst.*, vol. 27, 2014, pp. 1–16.

[9] M. Mirza and S. Osindero, "Conditional generative adversarial nets," 2014, *arXiv:1411.1784*.

[10] M. Arjovsky, S. Chintala, and L. Bottou, "Wasserstein generative adversarial networks," in *Proc. Int. Conf. Mach. Learn.*, 2017, pp. 214–223.

[11] A. Radford, L. Metz, and S. Chintala, "Unsupervised representation learning with deep convolutional generative adversarial networks," 2015, *arXiv:1511.06434*.

[12] J.-Y. Zhu, T. Park, P. Isola, and A. A. Efros, "Unpaired image-to-image translation using cycle-consistent adversarial networks," in *Proc. IEEE Int. Conf. Comput. Vis. (ICCV)*, Oct. 2017, pp. 2242–2251.

[13] V. Kukreja, D. Kumar, and A. Kaur, "GAN-based synthetic data augmentation for increased CNN performance in vehicle number plate recognition," in *Proc. 4th Int. Conf. Electron., Commun. Aerosp. Technol. (ICECA)*, Nov. 2020, pp. 1190–1195.

[14] G. Wang, W. Kang, Q. Wu, Z. Wang, and J. Gao, "Generative adversarial network (GAN) based data augmentation for palmprint recognition," in *Digital Image Computing: Techniques and Applications (DICTA)*. Piscataway, NJ, USA: IEEE Press, 2018, pp. 1–7.

[15] Y. Luo and B.-L. Lu, "EEG data augmentation for emotion recognition using a conditional Wasserstein GAN," in *Proc. 40th Annu. Int. Conf. IEEE Eng. Med. Biol. Soc. (EMBC)*, Jul. 2018, pp. 2535–2538.

[16] M. Patel, X. Wang, and S. Mao, "Data augmentation with conditional GAN for automatic modulation classification," in *Proc. 2nd ACM Workshop Wireless Secur. Mach. Learn.*, Jul. 2020, pp. 31–36.

[17] V. Sandfort, K. Yan, P. J. Pickhardt, and R. M. Summers, "Data augmentation using generative adversarial networks (CycleGAN) to improve generalizability in CT segmentation tasks," *Sci. Rep.*, vol. 9, no. 1, pp. 1–9, Nov. 2019.

[18] S. Motamed, P. Rogalla, and F. Khalvati, "Data augmentation using generative adversarial networks (GANs) for GAN-based detection of pneumonia and COVID-19 in chest X-ray images," *Informat. Med. Unlocked*, vol. 27, 2021, Art. no. 100779.

[19] A. Waheed, M. Goyal, D. Gupta, A. Khanna, F. Al-Turjman, and P. R. Pinheiro, "CovidGAN: Data augmentation using auxiliary classifier GAN for improved COVID-19 detection," *IEEE Access*, vol. 8, pp. 91916–91923, 2020.
[20] Q. H. Cap, H. Uga, S. Kagiwada, and H. Iyatomi, "LeafGAN: An effective data augmentation method for practical plant disease diagnosis," *IEEE Trans. Autom. Sci. Eng.*, vol. 19, no. 2, pp. 1258–1267, Apr. 2022.
[21] S.-W. Huang, C.-T. Lin, S.-P. Chen, Y.-Y. Wu, P.-H. Hsu, and S.-H. Lai, "AugGAN: Cross domain adaptation with GAN-based data augmentation," in *Proc. Eur. Conf. Comput. Vis. (ECCV)*, Sep. 2018, pp. 718–731.
[22] J. Lin, Y. Xia, T. Qin, Z. Chen, and T.-Y. Liu, "Conditional image-to-image translation," in *Proc. IEEE Conf. Comput. Vis. Pattern Recognit.*, Oct. 2018, pp. 5524–5532.
[23] Y. Lu, Y.-W. Tai, and C.-K. Tang, "Attribute-guided face generation using conditional CycleGAN," in *Proc. Eur. Conf. Comput. Vis. (ECCV)*, 2018, pp. 282–297.
[24] D. Manolakis, M. Pieper, E. Truslow, R. Lockwood, A. Weisner, J. Jacobson, and T. Cooley, "Longwave infrared hyperspectral imaging: Principles, progress, and challenges," *IEEE Geosci. Remote Sens. Mag.*, vol. 7, no. 2, pp. 72–100, Jun. 2019.
[25] D. Torbunov, Y. Huang, H. Yu, J. Huang, S. Yoo, M. Lin, B. Viren, and Y. Ren, "UVCGAN: UNet vision transformer cycle-consistent GAN for unpaired image-to-image translation," in *Proc. IEEE/CVF Winter Conf. Appl. Comput. Vis. (WACV)*, Jan. 2023, pp. 702–712.

JUNGJAE SON received the B.S. degree in electrical engineering from Pohang University of Science and Technology (POSTECH), Pohang, South Korea, in 2021. From June 2021 to May 2024, he was a Research Officer and a Lieutenant with the Chem-Bio Technology Center, Agency for Defense Development (ADD), Daejeon. He intends to pursue further research on integrated circuit design and deep learning with Korea Advanced Institute of Science and Technology (KAIST). His current research interests include LiDAR signal processing, algorithm design for chemical detection, and machine learning application technology.

HYUNG JOON BYUN (Graduate Student Member, IEEE) received the B.S. degree in electrical engineering from Ulsan National Institute of Science and Technology (UNIST), Ulsan, South Korea, in 2020. He is currently pursuing the Ph.D. degree with Cornell Tech, New York, NY, USA. From June 2020 to May 2023, he was a Research Officer and a Lieutenant with the Chem-Bio Technology Center, Agency for Defense Development (ADD), Daejeon. His current research interests include efficient 2.5D/3D integrated circuit design and hardware sustainability.

MUNYEOL PARK received the B.S. degree in electrical engineering from Pohang University of Science and Technology (POSTECH), Pohang, South Korea, in 2021. From June 2021 to May 2024, he was a Research Officer and a Lieutenant with the Chem-Bio Technology Center, Agency for Defense Development (ADD), Daejeon. He intends to pursue further research on artificial intelligence accelerator circuit design with Seoul National University (SNU). His current research interests include IR spectral analysis on a chemical gas cloud and model compression for deep neural networks.

JEONGJAE HA is currently pursuing the B.S. degree in chemical and biological engineering with Hanbat University, Daejeon, South Korea. Since 2021, he has been a Researcher with the Chem-Bio Technology Center, Agency for Defense Development (ADD), Daejeon. His current research interests include analysis of the chemical absorption spectrum and creating a standard chemical database for remote sensing.

HYUNWOO NAM (Member, IEEE) received the Ph.D. degree from the Electrical Engineering Department, Columbia University, in October 2016. He was with the Internet Real-Time Laboratory (IRT) under the supervision of Prof. H. Schulzrinne. He is currently a Senior Researcher with the Agency for Defense Development (ADD), South Korea. During the Ph.D. years, he collaborated with Bell Labs and Verizon, with a focus on capacity planning for wireless networks, analysis of adaptive bitrate streaming technologies, SDN and NFV for intelligent content delivery over wireless, and remote gas sensing systems. His research interests include the analysis of video streaming and intelligent content delivery over wireless networks.